Modelling Simul. Mater. Sci. Eng. 3 (1995) 597–613. Printed in the UK

# On the continuum versus atomistic descriptions of dislocation nucleation and cleavage in nickel

Peter Gumbsch† and Glenn E Beltz‡

† Max-Planck-Institut für Metallforschung, Institut für Werkstoffwissenschaft, D-70174 Stuttgart, Germany

‡ Department of Mechanical and Environmental Engineering, University of California, Santa Barbara, CA 93106-5070, USA

Received 12 February 1995, accepted for publication 11 May 1995

**Abstract.** A hybrid atomistic–finite-element model is compared with the continuum-based Peierls–Nabarro model for several crack orientations in a nickel crystal. Both methods incorporate the same embedded-atom potential for Ni, in order to make the comparison as valid as possible. The agreement (expressed in terms of a stability diagram showing envelopes in loading space where fracture or dislocation nucleation are likely to occur) is excellent in the case of a crack lying on a {111} plane, with a crack front running along a {211}-type direction, subject to mixed-mode I–II loadings. That orientation involves dislocation nucleation on the prolongation of the crack plane, and hence no ledge is formed upon dislocation nucleation. In other geometries considered (involving a crack on a {100}-type plane), the agreement seems to get poorer with increasing size of the ledge that is created when a dislocation nucleates. In all geometries, the atomistic model shows that incipient dislocation-like features are present before dislocation nucleation takes place, which serves as additional validation of the continuum Peierls–Nabarro model.

## 1. Introduction

In recent years, the competition between brittle fracture and plasticity at cracks in metallic crystals has been studied within two broad frameworks, namely from a continuum mechanics standpoint as well as an atomistic standpoint. Examples of the former date as far back as the model of Rice and Thomson [1], which sought to compare the Griffith cleavage load with the load required to make a pre-existing dislocation line ahead of a crack unstable, and models which evolved from that, which most recently are based on the Peierls–Nabarro model of a dislocation [2–6]. Furthermore, continuum modelling of the ductile versus brittle nature of materials is certainly not limited to models on the dislocation scale; an extensive literature exists on continuum plasticity theory applied to cracks in metals, and a relevant example includes the single-crystal plasticity theory of Saeedvafa and Rice [7, 8] applied to copper crystals.

Early examples of atomistic models used to study processes at a crack tip via computer simulation (see, e.g., [9–13]) exclusively made use of pair potentials to model the interatomic interaction. The availability of multibody interatomic potentials such as the embedded-atom method (EAM) due to Daw and co-workers [14–16] has made the atomistic approach even more attractive. To provide these models with realistic properties without excessive computational effort, the lattice region containing the crack tip can be embedded in a continuum. In earlier studies, the continuum was adapted to an analytical solution for the

0965-0393/95/050597+17$19.50  

stress field surrounding a crack [17]. A common difficulty with such a hybrid model is the proper treatment of the interface between the lattice and the continuum, especially if the interface is sought to respond flexibly to changes in atomic positions. The problem arises from the different nature of the internal forces which act in the two regions; in contrast with a classical ('local') continuum, internal forces in an atomistic region possess a finite range. Conceptually, the simplest way of producing a flexible boundary is to represent the continuum region by finite elements (FEs). In earlier FE models, the problem was dealt with by coupling several atoms to each element at the interface [12]. This causes force oscillations at the interface to cancel out, but the procedure tends to make the FE continuum unable to respond to local stress gradients. A more recent method of coupling the atomistic core region to a FE continuum has been published by Kohlhoff and co-workers [18, 19] that provides minimum disturbance at the interface. The model is commonly referred to as the FE model combined with atomistic modelling (FEAt) and will be described in further detail below.

Unfortunately, experimental work aimed at comparisons with the various models is still at an infant stage; aside from preliminary quantitative work by Ohr [20] and Chiao and Clarke [21], most experiments have been qualitative in nature, such as the investigation of directional cracking and segregation effects in copper bicrystals and copper–sapphire interfaces by Wang and co-workers [22, 23].

Even amongst the different models, little is known about their relationship. Aside from some initial comparative efforts by Thomson and co-workers [24–26], Sun and co-workers [27–29] and Hoagland and Heinisch [30], not much investigation has been done into the differences between the various models. The purpose of this paper is to provide a detailed comparison of results between the Peierls model, recently developed by Rice and co-workers [3–5, 27, 29] and Sun and Beltz [28], and atomistic calculations making use of the FEAt model developed by Kohlhoff *et al* [18, 19] and Gumbsch [31].

## 2. The combined finite-element–atomistic method

We briefly review the model developed by Kohlhoff *et al* [18, 19] and Gumbsch [31] that combines a lattice region and a continuum region via a transition zone. The continuum is described by linear elastic FEs. The atomistic region is modelled with an EAM potential for nickel given by Foiles *et al* [15]. The region in which the continuum and the lattice overlap provides a smooth transition between the atomistic core and the continuum region. Details of the coupling and the justification for the transition zone can be found in [19], where the transition is discussed in terms of Kröner's [32] 'non-local elasticity' theory.

A schematic outline of the model is depicted in figure 1. The outermost FE nodes are prescribed to the positions according to the anisotropic linear elastic solution for a sharp crack given by Sih and Liebowitz [33]. To guarantee that the system size is large enough to allow the application of linear elasticity at the outer border of the FE region, the required size of the model and the relative sizes of the atomistic and continuum regions have been determined by size scaling tests on the configuration described later as model A under pure mode I (opening) load [31]. We use about $70 \times 70$ lattice parameters for the total size of the model and about $10 \times 10$ lattice parameters for the atomistic region. Periodic boundary conditions of minimal length are applied along the crack front.

The determination of the critical loadings to failure, i.e. crack extension, retreat or dislocation emission is carried out as follows: for a given loading, characterized by the relative amounts of mode I, II and III loadings, we first determine the magnitude of the Griffith stress intensity factor $\tilde{K}_G$ such that the total energy release rate $G = G_I + G_{II} + G_{III}$

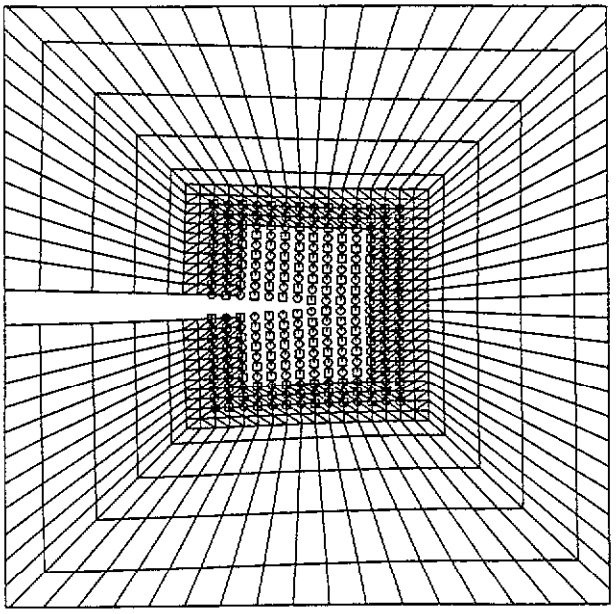

**Figure 1.** FEAt model of a crack tip in an FCC crystal. An atomistic zone is embedded in a continuum described by FEs; coupling is provided by a transition region consisting of two zones, as discussed in the text.

equals twice the surface energy. We then apply the displacements from the linear elastic solution for a load $\tilde{K} = \alpha \tilde{K}_G$ to all FE nodes and atoms, keeping the outermost FE nodes fixed at these positions and relax all other degrees of freedom of the whole model using a conjugate-gradient algorithm [34, 35] until the sum of the forces on all atoms and FE nodes falls below $10^{-6}$ eV Å$^{-1}$ (which results in very well converged models). We then vary $\alpha$, usually very close to unity, until we find a load $\tilde{K}$ at which the crack is stable. By that, we mean that the atomically sharp crack tip must stay at the position of the linear elastic crack field and must not heal, advance or emit dislocations. Doing so we can allow all atoms within interaction distance to interact and do not need to specify *a priori* which bonds are broken, which has introduced some kind of arbitrariness into earlier models [19]. Having found a stable configuration, we can use it as our starting point for further loading and unloading. This is possible in an atomistic model because, unlike a crack in a continuum, the crack in a discrete lattice can withstand a certain loading range until it becomes unstable. This effect is usually referred to as *lattice trapping* [36]. For the models discussed here, i.e. cracks in a close-packed FCC lattice and a rather 'soft' interatomic potential, the lattice trapping range $\Delta\alpha = \alpha^+ - \alpha^-$ is small and amounts to only a few per cent of $\alpha$. More details about the boundary conditions and the loading procedure have been given elsewhere [31].

It seems worthwhile pointing out that this method of loading an atomistic crack is in itself consistent with the outer boundary condition for an atomically sharp crack tip. We thereby deliberately restrict ourselves to geometries which can support an atomically sharp brittle crack, in order to avoid having to deal with ill-defined starting conditions. If the requirement of a stable crack as a starting point is relieved and the linear elastic continuum solution is directly used as a starting configuration, unrealistic results, such as Lomer dislocations at the

crack tip, are found [37, 38]. Furthermore, following this procedure allows us to approach criticality gradually and to analyse the critical configurations associated with both dislocation emission as well as brittle fracture much more precisely than by taking 'snapshots' of the emerging partial dislocations out of an unstable configuration as previously attempted [30].

We would also like to make one point regarding the anisotropic elastic formulation for the continuum quantities discussed in this paper that does not seem to receive wide attention in the literature: the anisotropic formulation considered here assumes that the $z$ axis (along the crack front) is perpendicular to a mirror plane of the lattice, so that the in-plane field quantities are decoupled from the antiplane quantities. If this is not true, the assumption that a mirror plane is present is only good as an approximation [28].

## 3. The Peierls–Nabarro framework

### *3.1. Basic features of the model*

Recent analyses of dislocation emission from a crack tip by Rice and co-workers [3–5, 27, 28] are based on the Peierls–Nabarro [39, 40] model of a straight-line dislocation. This model combines atomistic descriptions of the dislocation core with continuum elasticity in a physically realistic fashion and describes the process of a dislocation core nucleated from nil at a crack tip. Similarly to the Peierls–Nabarro model of a dislocation core, the nucleating incipient dislocation at a crack tip is depicted as follows: a distribution of discontinuity in the displacement field across the slip plane is assumed to obey a sinusoidal law of shear stress versus displacement and is embedded in a linear elastic medium surrounding the crack. The main advantage of the new approach is the elimination of the ill-defined dislocation core cut-off radius $r_c$ used by Rice and Thomson [1]. A physical property identified by Rice [4], the unstable stacking energy $\gamma_{us}$, is the key to the analysis of dislocation emission from a crack tip in the Peierls framework. Other parameters relating to the so-called 'tension–shear coupling' effect are included as well and replace $\gamma_{us}$ in more refined treatments. We note that the newer approach contains no account of the energy of the ledge formed at the crack tip by the emergent dislocation; however, one of the purposes of this paper is to speculate on its importance, in light of the FEAt results.

Additional reservations should be made here regarding the Peierls-type analysis for dislocation emission. Recent atomistic studies by Thomson and co-workers [24–26] indicate that the Peierls model may underestimate the critical loading for dislocation emission by as much as 50% when the slip plane is tilted with respect to the crack plane. The agreement of the two types of approach is good in the case of coplanar crack and slip planes. Whether the discrepancy is due to the discrete nature of the system, resulting in lattice trapping in the slip process, or the so-called ledge effect remains open for further research. Furthermore, we note that the Peierls model does not take into account stress-induced surface reconstructions, which may alter the predictions by the Peierls model and the Griffith cleavage condition.

Since all crystals are anisotropic and most existing atomistic simulations correspond to *anisotropic* crystals, the Peierls framework for dislocation emission in this paper will be based on work of Sun and Beltz [28] that incorporates anisotropic elasticity.

### *3.2. Integral equation formulation for combined tension and shear*

In its original form, Rice [4] showed analytically that, when a slip plane is a prolongation of a crack plane, the 'applied' energy release rate $G$ must attain the value of $\gamma_{us}$ for an incipient dislocation to become unstable and then to emit. This result is valid for general

anisotropic materials, provided that there is a pure edge dislocation under mode II loading, or a pure screw dislocation under mode III loading. Of more interest, however, are cases involving inclined slip planes and/or arbitrary Burgers vector orientations with respect to the dislocation line. An approximation to such problems would invoke the concept of effective stress intensity factors $K_\alpha^{eff}$ obtained by projecting relevant shear stresses onto the inclined plane and in the direction of the Burgers vector. This procedure has been described in detail by Sun and Beltz [28] and will not be used in this paper. Rather, we use an exact integral-equation treatment for the general case involving inclined slip planes and mixed edge and screw components, including tension–shear coupling.

Let us consider the general scenario: suppose that a slip plane intersects the crack plane, that the intersection line is also the crack front, and that the slip plane makes an angle $\theta$ with the crack plane. Assume that the crack tip is loaded by $(K_1, K_2, K_3) = (K_{II}, K_I, K_{III})$; the $K_\alpha$ here are the local (and screened) stress intensity factors near the crack tip. Assume that the crack does not extend. The stress concentration near the crack tip is relieved by an emergent zone of displacement discontinuity $\{\delta_r(r), \delta_\theta(r), \delta_z(r)\}$ across the slip plane, i.e. an incipient dislocation. The incipient slip zone is illustrated in figure 2.

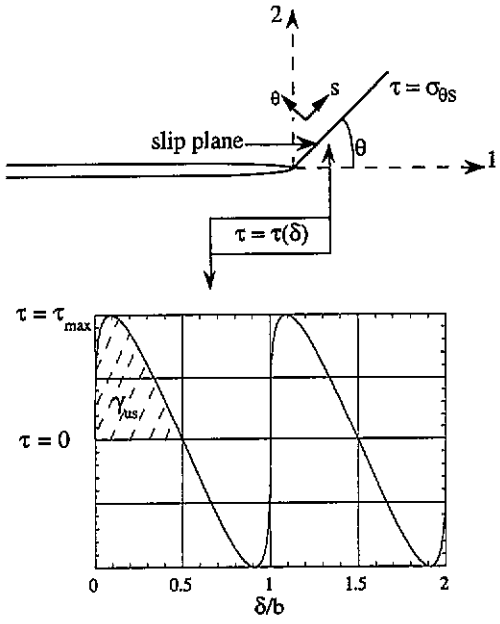


**Figure 2.** An incipient dislocation, represented by a distribution of sliding and opening displacement, develops along a slip plane inclined at angle $\theta$ with respect to the crack plane in response to mixed-mode loading prescribed by $K_I$ and $K_{II}$. A periodic relation is assumed to relate the shear stress and the sliding discontinuity in the continuum modelling.

The edge slip direction is along $r$, the normal direction is along $\theta$ with the unit directional vector $n$, and the screw slip direction is along $z$. The edge component is $\delta_r(r) = u_r^+(r) - u_r^-(r)$ and the screw component $\delta_z(r) = u_z^+(r) - u_z^-(r)$; the discontinuity in the opening direction $\delta_\theta(r) = u_\theta^+(r) - u_\theta^-(r) = n_\alpha[u_\alpha^+(r) - u_\alpha^-(r)]$. The slip direction in the slip plane has the unit directional vector denoted $s = (\cos\phi, 0, \sin\phi)$ in the $r, \theta, z$ coordinate system. The sign convention for the angle $\phi$ of the slip direction is that $\phi$ is defined as positive when the slip direction rotates from the $r$ axis toward the $z$ axis. The displacement discontinuity across the slip plane in that direction is $\delta_s(r) = s_\alpha\delta_\alpha(r) = s_\alpha[u_\alpha^+(r) - u_\alpha^-(r)]$. The incipient profile $\delta_\alpha(s)$ is modelled here as a continuous distribution of an individual dislocation at location $s$ of an infinitesimal Burgers vector

$$db_\alpha = \left[-\frac{d\delta_\alpha(s)}{ds}\,ds\right] \tag{1}$$

which in turn will exert stresses

$$\sigma_{\theta\alpha}(r) = g_{\alpha\beta}(r, s; \theta)\left[-\frac{\mathrm{d}\delta_\beta(s)}{\mathrm{d}s}\,\mathrm{d}s\right] \tag{2}$$

on a point $r$ along the slip plane. The Green functions $g_{\alpha\beta}(r, s; \theta)$ so defined can be obtained by solutions of a line dislocation interacting with the crack tip in the anisotropic linear elastic medium [28]. It can be shown that the Green functions $g_{\alpha\beta}(r, s; \theta)$ can be expressed in the form

$$g_{\alpha\beta}(r, s; \theta) = \frac{1}{4\pi}\sqrt{\frac{s}{r}}\frac{[\Lambda_{\alpha\beta}^{-1} + h_{\alpha\beta}(r/s, \theta)]}{r - s} \tag{3}$$

where $8\pi\Lambda_{\alpha\beta}$ is the inverse of the pre-logarithmic matrix appearing in the expression for the energy of a straight dislocation line positioned along a crack front. Following anisotropic elastic crack theory [33], the Irwin formula for $G$, the elastic energy release rate, is $G = K_\alpha \Lambda_{\alpha\beta} K_\beta$. Further details regarding the stress functions $g_{\alpha\beta}(r, s; \theta)$ and $h_{\alpha\beta}(r, s; \theta)$ may be found in [28].

The force balance at a material point $r$ along the slip plane gives the following equation of equilibrium:

$$\sigma_{\theta\alpha}[\delta(r)] = \sigma^0_{\theta\alpha}(r) + \int_0^\infty g_{\alpha\beta}(r, s, \theta)\left[-\frac{\mathrm{d}\delta_\beta(s)}{\mathrm{d}s}\,\mathrm{d}s\right] \tag{4}$$

where $(\alpha, \beta) = (r, \theta, z)$ which is also denoted as $(1, 2, 3)$, and $\sigma^0_{\theta\alpha}(r)$, the unrelaxed stresses from the crack loading $K_\alpha$, are given as $\sigma^0_{\theta\alpha}(r) = F_{\alpha\beta}(\theta)K_\beta/\sqrt{2\pi r}$. The functions $F_{\alpha\beta}(\theta)$ give the angular dependence of the linear elastic asymptotic stress field around a crack in an anisotropic body and are derived and conveniently tabulated in [33]. The term $\sigma_{\theta\alpha}[\delta_\gamma(r)]$ is the lattice-restoring shear and tension stress against the displacement discontinuities across the slip plane at point $r$, with which a potential $\Phi[\delta_\alpha(r)]$ is associated, such that

$$\sigma_{\theta\alpha}[\delta(r)] = \frac{\partial\Phi[\delta(r)]}{\partial\delta_\alpha(r)}. \tag{5}$$

Equations (4) and (5) constitute a complete set of equations which may be solved simultaneously by numerical methods.

We also apply the constrained slip path approximation here. Let the slip be constrained to the direction $s$ (the same as $b$) that makes an angle $\phi$ with the $r$ axis in the slip plane, $\delta_\alpha(r) = [\delta_s(r)\cos\phi, \delta_\theta(r), \delta_s(r)\sin\phi]$ and the stress $\tau = \sigma_{\theta r}\cos\phi + \sigma_{\theta z}\sin\phi$ and $\sigma = \sigma_{\theta\theta}$. We seek the condition under which the profile becomes unstable, after which a dislocation can emerge and move away from the crack tip until it is stopped by the lattice resistance, by the Peierls stress $\sigma_\pi$ or by interaction with distant dislocations. We obtain the following equations:

$$\tau[\delta_s(r), \delta_\theta(r)] = \frac{K_\tau^{eff}}{\sqrt{2\pi r}} - \int_0^\infty \bar{g}_{11}(r, s; \theta, \phi)\frac{\mathrm{d}\delta_s(s)}{\mathrm{d}s}\,\mathrm{d}s - \int_0^\infty \bar{g}_{12}(r, s; \theta, \phi)\frac{\mathrm{d}\delta_\theta(s)}{\mathrm{d}s}\,\mathrm{d}s \tag{6}$$

$$\sigma[\delta_s(r), \delta_\theta(r)] = \frac{K_\sigma^{eff}}{\sqrt{2\pi r}} - \int_0^\infty \bar{g}_{21}(r, s; \theta, \phi)\frac{\mathrm{d}\delta_s(s)}{\mathrm{d}s}\,\mathrm{d}s - \int_0^\infty \bar{g}_{22}(r, s; \theta, \phi)\frac{\mathrm{d}\delta_\theta(s)}{\mathrm{d}s}\,\mathrm{d}s \tag{7}$$

where

$$K_\tau^{eff} = \sqrt{2\pi r}[\cos\phi\sigma^0_{\theta r}(r, \theta) + \sin\phi\sigma^0_{\theta z}(r, \theta)] = s_\alpha(\phi)F_{\alpha\beta}(\theta)K_\beta \tag{8}$$

and

$$K_\sigma^{eff} = \sqrt{2\pi r}\sigma_{\theta\theta}^0(r,\theta) = F_{2\beta}(\theta)K_\beta. \tag{9}$$

These are defined for the singular stresses $\sigma_{\theta r}^0$, $\sigma_{\theta z}^0$ and $\sigma_{\theta\theta}^0$ at the crack tip under external loading before the emergence of the incipient profile. The functions $\bar{g}_{11}$, $\bar{g}_{12}$, $\bar{g}_{21}$ and $\bar{g}_{22}$ are stress functions for a straight dislocation at a crack tip:

$$\bar{g}_{11}(r,s;\theta) = s_\alpha(\phi)g_{\alpha\beta}(r,s;\theta)s_\beta(\phi) \tag{10a}$$

$$\bar{g}_{12}(r,s;\theta) = s_\alpha(\phi)g_{\alpha 2}(r,s;\theta) \tag{10b}$$

$$\bar{g}_{21}(r,s;\theta) = g_{2\alpha}(r,s;\theta)s_\alpha(\phi) \tag{10c}$$

$$\bar{g}_{22}(r,s;\theta) = g_{22}(r,s;\theta). \tag{10d}$$

All these terms and functions can be obtained from the singular field of a loaded crack tip and from the solution for a dislocation near a crack tip using anisotropic elasticity theory [41–43].

The terms $\tau[\delta_s(r),\delta_\theta(r)]$ and $\sigma[\delta_s(r),\delta_\theta(r)]$ are lattice-restoring shear and tension stresses against the displacement discontinuities across the slip plane; a potential $\Phi[\delta_s(r),\delta_\theta(r)]$ is assumed to exist, such that

$$\tau[\delta_s(r),\delta_\theta(r)] = \frac{\partial\Phi[\delta_s(r),\delta_\theta(r)]}{\partial\delta_s(r)} \tag{11}$$

$$\sigma[\delta_s(r),\delta_\theta(r)] = \frac{\partial\Phi[\delta_s(r),\delta_\theta(r)]}{\partial\delta_\theta(r)}. \tag{12}$$

Modelling of the constitutive law $\Phi[\delta_s(r),\delta_\theta(r)]$ from EAM results for Ni, Al, $Ni_3Al$ and Fe, and from density functional studies of Si has been provided by Sun *et al* [27] in the form of an analytical representation, which is discussed further by Beltz and Rice [3, 5]. The form for nickel, based on the EAM results of Foiles *et al* [15] and which may be found explicitly in [27], is used for the calculations discussed in this paper. Equations (6)–(12) constitute a complete set of equations which can be solved simultaneously to determine the critical loading and the corresponding incipient configuration. The solutions are obtainable numerically, by use of the Newton–Raphson method and Chebyshev polynomials of the second kind (see, e.g., Beltz and Rice [5] and Erdogan and Gupta [44]).

### *3.3. The shear-only model*

In a shear-only model, where only slip displacements and shear stresses are considered, a simpler set of equations exists:

$$\tau[\delta_s(r)] = \frac{K_\tau^{eff}}{\sqrt{2\pi r}} - \int_0^\infty \bar{g}_{11}(r,s;\theta,\phi)\frac{\mathrm{d}\delta_s(s)}{\mathrm{d}s}\,\mathrm{d}s. \tag{13}$$

Equation (13) is accompanied by a sinusoidal law

$$\tau(\Delta_s) = (\pi\gamma_{us}/b)\sin(2\pi\Delta_s/b) \tag{14}$$

where $\Delta_s$ is the relative atomic sliding displacement between the two adjacent slipping atomic layers, which is related to $\delta_s$, the displacement discontinuity across the slip plane, by

$$\delta_s = \Delta_s - (b/2\pi)\sin(2\pi\Delta_s/b). \tag{15}$$

## 4. Model geometries for comparison

Two orientations of nickel, together with two schemes for mixed-mode loading, are chosen to give three situations for comparison in this study. For later convenience, we denote them with letters as follows. Orientation A consists of a crack on the (100) plane, with the crack front running along the [011] direction. The crack propagation direction is thus $[01\bar{1}]$. The crack is oriented such that the crack plane intersects {111}-type slip planes along the crack front, at angles of $\pm 54.7°$ (or $\pm 125.3°$). Furthermore, since the (011) plane is a mirror plane in the FCC structure, the anisotropic elastic formulation used here is exact. The loadings considered are predominantly mode I: however, we vary the relative amounts of mode II or mode III components. It is common in the fracture literature to define a phase angle $\Psi$ such that

$$\tan \Psi = K_{II}/K_I \qquad \text{or} \qquad \tan \Psi = K_{III}/K_I \tag{16}$$

depending on which loading mixture is under consideration. Hence, $\Psi = 0°$ corresponds to pure mode I, while increasing $\Psi$ signifies increasing mode mixity.

Orientation B consists of a crack on the (111) plane, with the crack front running along the $[2\bar{1}\bar{1}]$ direction. The crack propagation direction is again $[01\bar{1}]$. The crack tip is oriented such that the only intersecting {111}-type slip plane is the crack plane itself. Here, the Peierls–Nabarro type of analysis has the feature that it reproduces a fracture process for cases when cleavage is favoured [3, 27]. This orientation has the slight drawback that, since {211} planes are *not* mirror planes in the FCC structure, the anisotropic elasticity formulation is at best an approximation. Since this approximation is expected to become less accurate as out-of-plane loadings are added, we consider only mixed-mode I–II loading for orientation B.

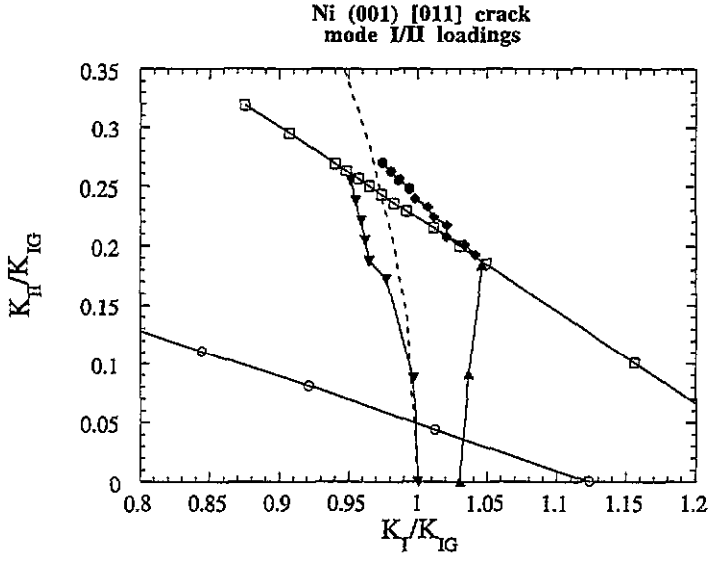


**Figure 3.** Stability diagram for a Ni (001) [011] crack subject to mixed-mode I–II loadings. Circles represent dislocation nucleation, triangles denote the stability envelope for the main crack, and diamonds and squares indicate cleavage on the inclined (−54.7°) plane. Furthermore, open symbols originate from the Peierls–Nabarro continuum model and closed symbols are from the FEAt model. The broken line represents the Griffith cleavage condition.

## 5. Results and discussion

### *5.1. Orientation A; mode I–II loadings*

A 'stability' diagram, showing the envelope (in $K_I$–$K_{II}$ space) where cleavage or dislocation nucleation has not occurred yet, is shown in figure 3. Both axes are normalized to $K_{IG}$, the value of needed for Griffith cleavage under pure mode I conditions. Inherent in the atomistic results is a finite range of stress intensity factors for a given phase angle, below which crack healing would occur, and above which the crack would continue to extend. The atomistic results show three distinct regimes. Below a phase angle of approximately 10°, the failure mode is cleavage along the (100) plane, i.e. the original crack plane. Between 10° and 15°, the failure mode is cleavage along a {111}-type plane inclined at −54.7° with the original crack plane. At larger phase angles, the failure occurs by the emission of a Shockley partial dislocation of pure edge type (i.e. $\phi = 0$) on the {111}-type plane at −125.3°.

As expected, the Peierls–Nabarro type of analysis applied to the slip planes inclined at +54.7° and +125.3° gives energy release rates at instability that are large compared with $G$ for Griffith crack propagation; hence, these possibilities are not considered further. For the time being, consider the possibility that an instability occurs on the plane at −54.7°. The Peierls–Nabarro result predicts that $G$ for this instability drops below the Griffith cleavage value at a phase angle of 14°, which is in very good agreement with the FEAt model. This possibility for cleavage on the inclined plane assumes that dislocation nucleation is suppressed on the plane at −125.3° and is only mentioned to illustrate that fracture-like instabilities on planes other than the crack plane are in excellent agreement with the atomic model. A coupled Peierls–Nabarro solution cannot be applied to the slip plane at −125.3°, because the potentials in [27] lose their validity for cases involving relatively small amounts of tension, or compression, acting across the slip plane. This is aggravated by numerical problems associated with the lack of a precise physical meaning of $\delta_\theta$ when it becomes negative. Hence, for this case, a shear-only type analysis is considered. As seen in figure 3, dislocation emission (of an edge-type Shockley partial) on the plane at −125.3° becomes favourable when the phase angle is increased beyond approximately 2°. This is in stark contrast with the atomistic model, which predicts that the dislocation emits at much larger phase angles and therefore at much higher effective shear stress intensities on the glide plane.

### *5.2. Orientation A; mode I–III loadings*

The loading diagram for this case, showing $K_I$–$K_{III}$ space, is shown in figure 4(*a*). The atomistic model predicts that cleavage occurs along the (100) crack plane for phase angles below approximately 7°. For larger amounts of mode III loading, the failure mode is emission of a partial dislocation on the plane inclined at 54.7° to the crack plane (due to the symmetry of this situation, this could occur at ±54.7°). This Shockley partial dislocation is mixed, i.e. $\phi = 60°$. Note that there still is a finite 'trapping' range when cleavage dominates, i.e. there is a range of loadings between which the crack neither extends nor heals.

The Peierls–Nabarro model gives a transition phase angle of approximately 4°, i.e. 3° less than that predicted by the atomistic model. The corresponding effective values $K_\tau^{eff}$ of $K_{II}$ at dislocation nucleation are 0.206 MPa $m^{1/2}$ in the FEAt model and 0.166 MPa $m^{1/2}$ in the Peierls–Nabarro model. The agreement, while markedly better than in the previous case involving mode II loadings and a pure edge dislocation, is still only moderate.

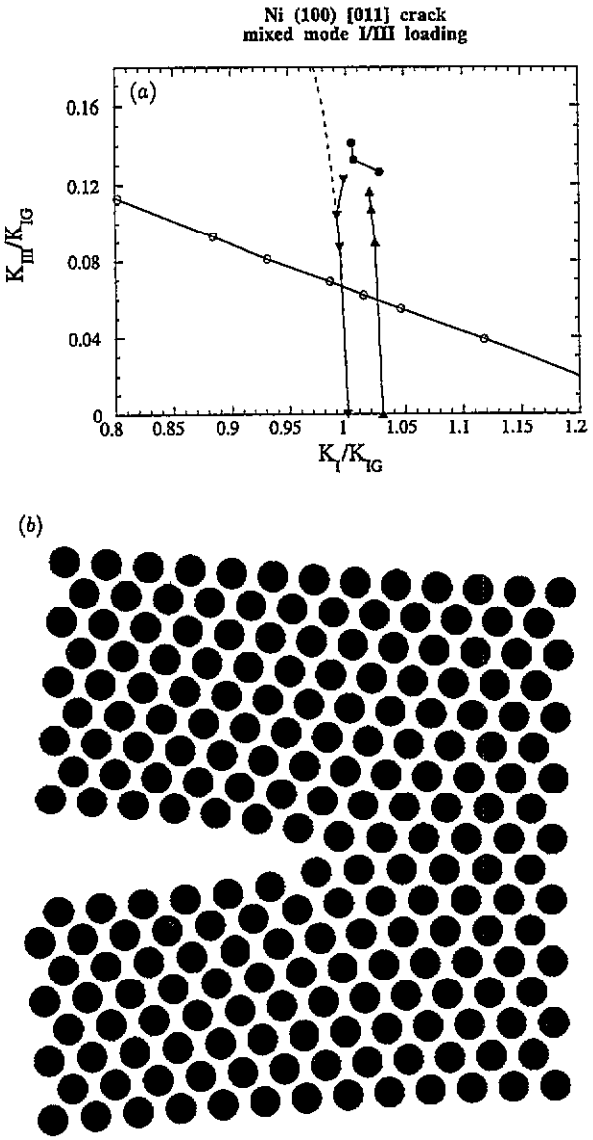


**Figure 4.** (*a*) Stability diagram for a Ni (001) [011] crack subject to mixed-mode I–III loadings. Circles represent dislocation nucleation and triangles denote the stability envelope for the main crack. Open symbols are from the Peierls–Nabarro continuum model and full symbols are from the FEAt model. (*b*) Atomic positions prior to instability in the same crack.

One remark should be made about the actual crack tip geometry of the (100) [011] crack displayed in figure 4(*b*). The precise atomistic 'position' of the crack tip can be such that the last intact bond connects atoms from the upper left to the lower right of the crack tip, which we usually chose, or vice versa. The atom movements for dislocation emission in mixed-mode I–III loading at the transition from brittle cleavage to dislocation emission always involve the breaking of this bond. Therefore, the dislocation on the (111) glide plane inclined at ±54.7° with respect to the crack plane is generated on the (111) plane *just ahead* of the crack tip. This poses the question of whether a crack tip position associated with the last bond connecting the atoms at the upper and the lower left of the crack tip (i.e. a crack with one more bond closed) would behave any differently. We therefore repeated the calculations under mixed-mode I–III loading with crack tips moved backwards by $a_0/4$ in order to study the effect. The resulting stability regime was identical with the original

regime (figure 4(*a*)) except for the point where dislocation emission occurs first. This point was shifted to 1% lower loads and the atom movements upon failure indicate that the additional connected bond first opened and, upon opening of the second bond (i.e. the crack tip bond of the original model), the dislocation was formed and emitted. Due to the negligibly small differences in both the critical load to failure and the qualitative failure behaviour we conclude that the precise location of the crack tip is not important for this crack system.

In figure 5 the relative atomic shear and opening quantities from the FEAt description of nickel are displayed. As noted in section 3.2, $\Delta$ refers to a relative atomic displacement (normal to the slip plane denoted $\Delta_\theta$, and parallel to the slip plane in the direction of the Burgers shear displacement denoted $\Delta_s$). Moreover, the $\delta$ quantities refer to a displacement discontinuity across the slip plane, which can be viewed as the non-linear contributions that result when the displacements according to the linear elastic solution for the sharp crack tip are subtracted from $\Delta$. For each quantity, the results are plotted for the two separate (but equivalent) slip systems at $\pm 54.7°$. Although there is in principle symmetry, only one plane undergoes dislocation nucleation (the left diagrams) owing to an immediate relaxation of stresses due to the dislocation. These quantities are shown just prior to the instability for various phase angles (this corresponds to Griffith cleavage for phase angles less than 7°); in addition, the profile is shown just following dislocation nucleation in the case of $\Psi = 7°$. It is evident that the atomistic displacement results suggest that incipient dislocation-like features are present before dislocation nucleation takes place, which serves as additional validation of the continuum Peierls–Nabarro model. Since these displacement profiles tend to vary rapidly as the critical load for instability is reached, it is rather difficult to compare the profiles to the Peierls–Nabarro results; the situation is aggravated since the actual critical instability loads differ in this case between the two models. Hence, we defer comparison of displacement results to the next example.

### *5.3. Orientation B; mode I–II loadings*

As already mentioned, this orientation has the feature that the slip plane of interest is also the crack plane. The stability diagram is shown in figure 6. There is a very good agreement between the Peierls–Nabarro and atomistic models in this case; the critical ratios of $K_I$ to $K_{II}$ associated with the change from brittle to ductile behaviour are virtually the same in the two models; they differ by approximately 1°. Additionally, the effective $K$-values at dislocation nucleation are 0.175 MPa $m^{1/2}$ and 0.181 MPa $m^{1/2}$ for the FEAt and Peierls models, respectively.

Overall, the findings presented thus far suggest that the extent of the agreement between the two models can be understood, in part, by consideration of the 'ledge', or the free surface created when a dislocation emits from a surface or a crack tip. The Peierls–Nabarro framework for dislocation formation and emission at a crack has never satisfactorily included an account of the energy formed at such an atomic-scale ledge. Physically, it would seem reasonable that this added energetic term would tend to restrict dislocation nucleation, i.e. the Peierls–Nabarro model, as it stands, ought to *underestimate* the critical load for emission. Indeed, with the exception of the (111) crack used in the third example, that seems to be the case for the systems studied in this paper. The prospects for future modelling of the ledge effect are discussed as part of the following section.

Finally, comparisons of slip profiles at instability are given in figure 7. The various models are qualitatively similar in that the FEAt model does suggest that incipient features slowly build up prior to instability, and that the 'width' of the shear features prior to

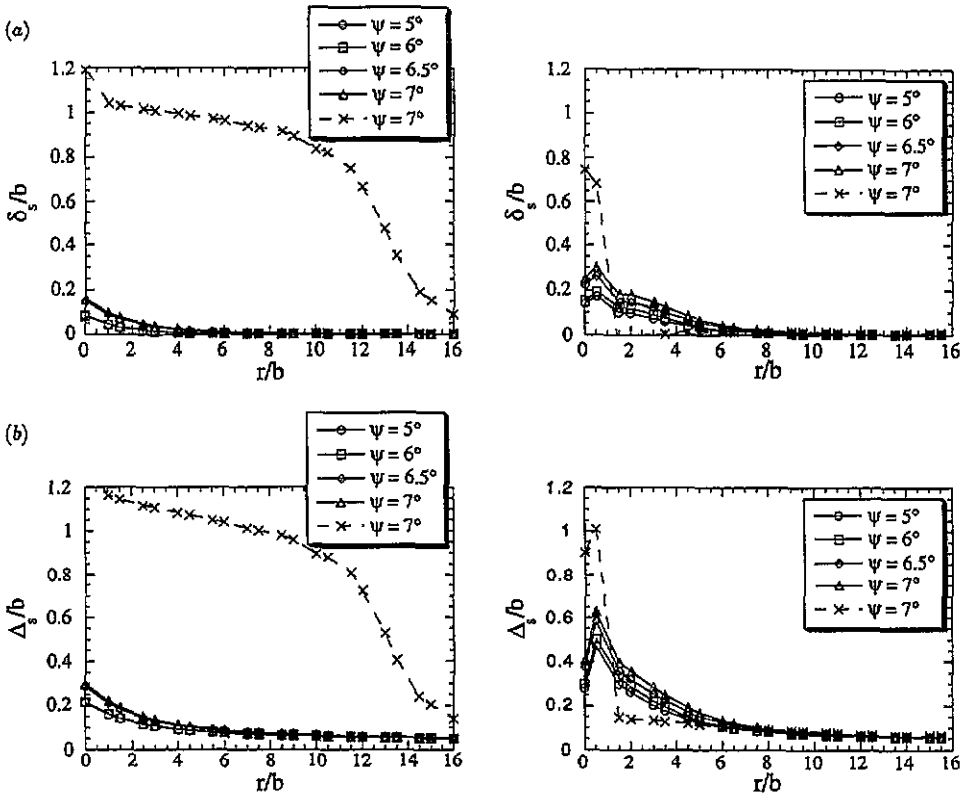


**Figure 5.** (*a*) Shear discontinuity profile $\delta_s(r)$ at the onset of unstable behaviour for symmetrically located planes inclined at ±54.7° (+, left; −, right) in the (001) [011] orientation. The phase angle denotes mode I–III mixity. All results are taken from the FEAt model. Dislocation nucleation on the plane at +54.7° occurs for phase angles greater than 7°, as indicated by the results just prior to and subsequent to emission. (*b*) Relative atomic sliding $\Delta_s(r)$ at onset of unstable behaviour for symmetrically located planes inclined at ±54.7° in the (001) [011] orientation (mode I–III loading). (*c*) Opening discontinuity profile $\delta_\theta(r)$ at onset of unstable behaviour for symmetrically located planes inclined at ±54.7° in the (001) [011] orientation (mode I–III loading). (*d*) Relative atomic opening $\Delta_\theta(r)$ at onset of unstable behaviour for symmetrically located planes inclined at ±54.7° in the (001) [011] orientation (mode I–III loading).

dislocation nucleation is of the order of several atomic spacings. Quantitative comparison is difficult, however, because these displacements strongly depend on loading near the instability point.

### *5.4. Enhancements to the models*

The Peierls treatment has the primary advantage over earlier dislocation emission models in that it does *not* consider an already-formed dislocation, i.e. it gives a realistic physical description (in two dimensions) of the actual nucleation of a dislocation at a crack. However, when the model is used to actually evaluate the ductile versus brittle behaviour of materials, such as for nickel in this paper, it must be realized that much more is occurring. The model does not take into account other processes which occur on various length scales away from the crack. These include but are not limited to incipient dislocation activity on competing

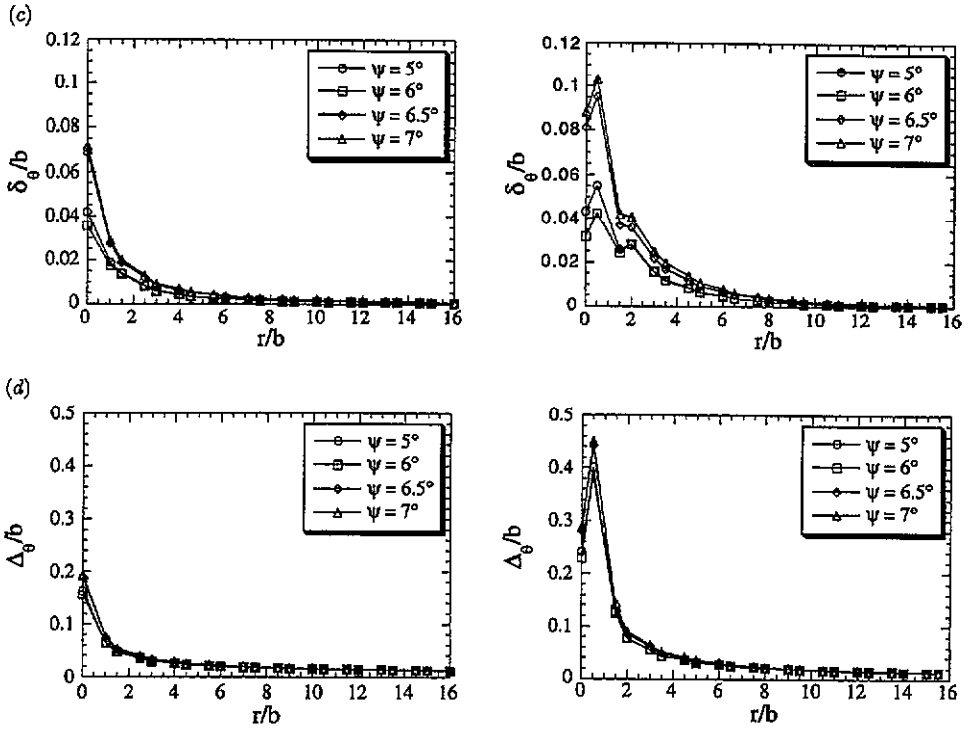


**Figure 5.** (Continued)

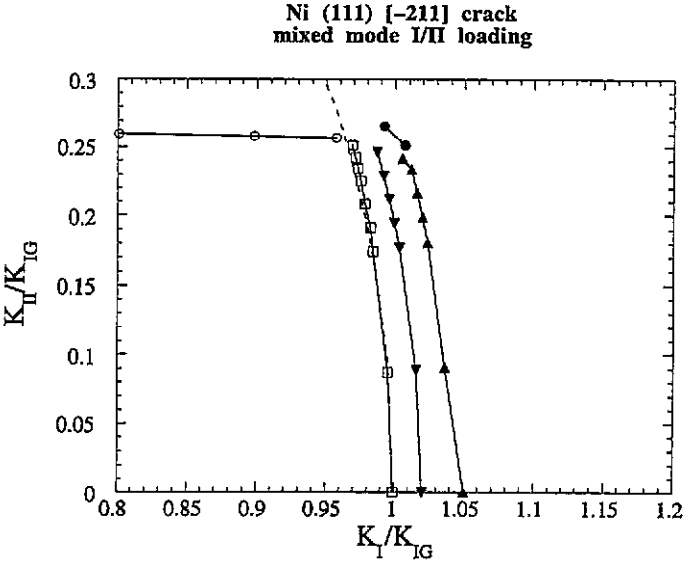


**Figure 6.** Stability diagram for a Ni (111) [$\bar{2}$11] crack subject to mixed-mode I–II loadings. Circles represent dislocation nucleation and all other shapes correspond to various cleavage modes. Open symbols are from the Peierls–Nabarro continuum model and full symbols are from the FEAt model.

slip planes at the crack tip, fully formed dislocations in various arrangements and distances from the crack, other defects such as boundaries and point defects, dislocation mobility, three-dimensional aspects, such as the (physically realistic) nucleation of dislocation loops, and other material inhomogeneities. Continuum models that remove many of the above

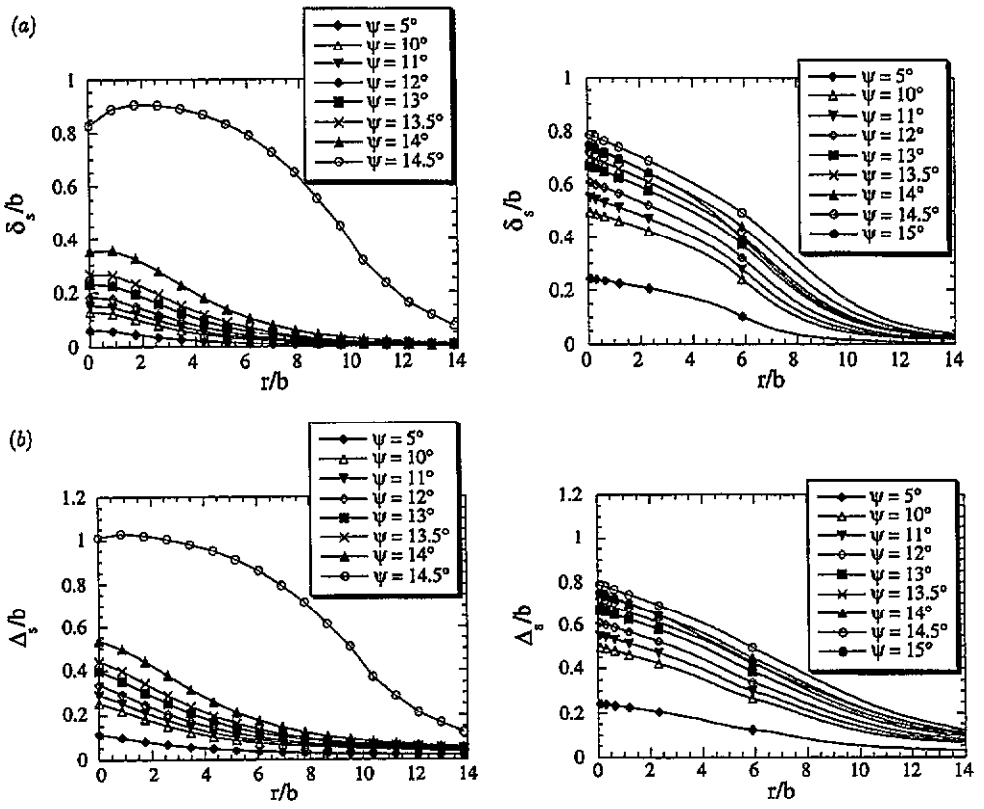


**Figure 7.** (*a*) Shear discontinuity profile $\delta_s(r)$ at onset of unstable behaviour for a slip plane located at 0° (FEAt model, left; Peierls model, right) in the (111) [$\bar{2}$11] orientation. The phase angle denotes mode I–II mixity. Relative atomic sliding $\Delta_s(r)$ at onset of unstable behaviour for a slip plane located at 0° (FEAt model, left; Peierls model, right) in the (111) [$\bar{2}$11] orientation. The phase angle denotes mode I–II mixity.(*c*) Opening discontinuity profile $\delta_\theta(r)$ at onset of unstable behaviour for a slip plane located at 0° (FEAt model, left; Peierls model, right) in the (111) [$\bar{2}$11] orientation. The phase angle denotes mode I–II mixity. (*d*) Relative atomic opening $\Delta_\theta(r)$ at onset of unstable behaviour for a slip plane located at 0° (FEAt model, left; Peierls model, right) in the (111) [$\bar{2}$11] orientation. The phase angle denotes mode I–II mixity.

assumptions are currently under consideration [45–48], and some of them are discussed in this section.

*5.4.1. Multiple-slip-plane effects.* The issue of incipient dislocation activity on planes *other* than the nucleation plane was addressed by Beltz and Schmauder [49]. A mathematical model that accounts for two slip planes (inclined at different angles with respect to the crack plane) was presented, and preliminary results for nickel indicated that incipient shear and/or opening discontinuities on slip planes other than the primary plane did not significantly affect the critical load for dislocation nucleation. For example, in a Peierls–Nabarro model for nickel that incorporated the same slip potential as in this paper, the critical load to nucleate a dislocation under mode I loading was determined when firstly the only slip or opening discontinuity permitted consisted of a {111} plane inclined at 70.53° and secondly, in addition to the plane at 70.53°, displacement discontinuities were allowed to develop along another {111} plane that was the prolongation of the crack (0°). The nucleation load

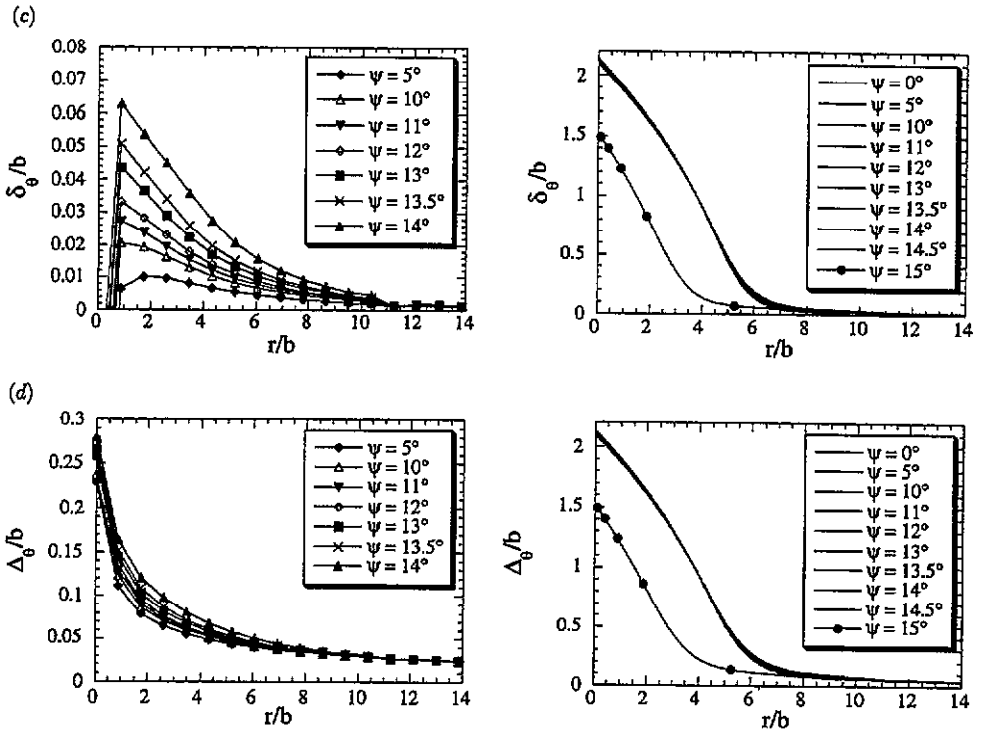


**Figure 7.** (Continued)

along another {111} plane that was the prolongation of the crack (0°). The nucleation load in the multiplane model was found to be approximately 8% larger. Whether this weak 'shielding' effect is important in other orientations has yet to be investigated; however, it seems reasonable to assume that it would never exceed 8–10% for typical orientations. Of course, interactions of all possible failure planes are already taken into account in the atomistic model.

*5.4.2. The ledge effect.* Another phenomenon already mentioned in this paper, and the subject of much debate, is the effect of the ledge that is formed when a dislocation is emitted from the crack tip region. As with multiple-slip-plane effects, the ledge effect is explicitly treated in the atomistic model but is completely ignored by the Peierls–Nabarro model. The results of this paper suggest that the Peierls modelling could benefit by accounting for the ledge energy, at least in cases involving the production of a relatively large step (e.g. large edge components of $b$ on an inclined slip plane. At first glance, one might attempt to add an energy term that depends linearly on the slip at the crack tip; unfortunately, that has the effect of introducing a Dirac singular term into the force balance implied by equation (6a) or (13). Several procedures for overcoming this difficulty have been proposed. The apparent singularity in force can be avoided by introducing a weighting function as a measure of displacement [50] or alternatively by use of a lattice-restoring force that varies from steady state as a crack or free surface is approached [29]. Additionally, Schoeck [51] has described a method that incorporates the ledge energy into the energetics of Peierls–Nabarro dislocation formation at cracks. Ultimately, the most physically realistic continuum-based description of the ledge effect may be based on a Peierls–Nabarro treatment of a dislocation core ahead

of a continually blunting crack, a problem currently under consideration [52, 53]. These formulations have not yet evolved to the state where detailed comparison with atomistic models for a particular material can be undertaken.

*5.4.3. Temperature effects.* The analyses of dislocation nucleation presented in this paper rigorously hold true at 0 K, i.e. thermal effects are neglected, except possibly through a weak temperature dependence of the elastic constants that enter the analysis. The FEAt model could be modified to account for temperature by utilizing molecular dynamics, rather than statics, in the inner atomistic region. The Peierls framework can also be modified to account for temperature by making use of an activation energy concept; the problem reduces to that of finding a 'saddle-point' configuration of slip, and calculating the difference in energy between the activated state and a pre-nucleation state. Such calculations have been carried out in two dimensions by Rice and Beltz [45] and Xu *et al* [46]. To be realistic, however, the thermal activation process is inherently three dimensional and so would be expected to take place over a localized region (in the form of a dislocation loop that jumps out). For simple slip geometries, the three-dimensional problem has been analysed in detail in an approximate fashion by Rice and Beltz [45], Schoeck and Püschl [54], and more exactly by Xu *et al* [46].

## 6. Summary

We have demonstrated that a basic premise for continuum models of dislocation nucleation and crack propagation based on the Peierls–Nabarro model is valid, namely, that stable incipient slip- and/or opening-like features are formed prior to instability. For the specific case of nickel, reasonably good agreement (in terms of loadings associated with dislocation nucleation or crack propagation) between the Peierls model and the FEAt model is attained provided that orientations are considered which involve the creation of relatively small ledge areas when a dislocation nucleates and emits. The presence of the ledge retards dislocation nucleation; hence, in those cases, the Peierls model underestimates critical loadings for nucleation compared to the FEAt model.

## Acknowledgments

GEB would like to acknowledge support from the Alexander von Humboldt Foundation, making a stay at the Max-Planck-Institut für Metallforschung in Stuttgart possible, as well as the Academic Senate Committee on Research at the University of California, Santa Barbara. PG acknowledges support from Deutsche Forschungsgemeinschaft. Discussions with Dr Yuemin Sun and Dr Robb Thomson, as well as Professor James R Rice and Professor Rob Phillips are appreciated. Finally, GEB would like to acknowledge the encouraging words of Professor A E Romanov during the final stages of the work.

## References

[1] Rice J R and Thomson R 1974 *Phil. Mag.* **29** 73

[2] Sun Y, Rice J R and Truskinovsky L 1991 *High-Temperature Ordered Intermetallic Alloys (Mater. Res. Soc. Symp. Proc. 213) (Boston, MA, 1990)* ed L A Johnson, D T Pope and J O Stiegler (Pittsburgh, PA: Materials Research Society) p 243

[3] Beltz G E and Rice J R 1991 *Modeling the Deformation of Crystalline Solids: Physical Theory, Application, and Experimental Comparisons, Proc. ASM–AIME Symp. ASM–TMS Spring Meeting (New Orleans, LA,*

*1991)* ed T C Lowe, A D Rollett, P S Follansbee and G S Daehn (Warrendale, PA: Metallurgical Society of AIME) p 457
[4] Rice J R 1992 *J. Mech. Phys. Solids* **40** 239
[5] Beltz G E and Rice J R 1992 *Acta Metall.* **40** S321
[6] Schoeck G 1991 *Phil. Mag.* A **63** 111
[7] Saeedvafa M and Rice J R 1992 *Mech. Mater.* **13** 295
[8] Saeedvafa M and Rice J R 1992 *Modelling Simul. Mater. Sci. Eng.* **1** 53
[9] Gehlen P C 1973 *Scr. Metall.* **7** 1115
[10] Sinclair J E 1975 *Phil. Mag.* **31** 647
[11] Markworth A J, Kahn L R, Gehlen P C and Hahn G T 1981 *Res. Mech.* **2** 141
[12] Mullins M and Dokainish M A 1982 *Phil. Mag.* A **46** 771
[13] deCelis B, Argon A S and Yip S 1983 *J. Appl. Phys.* **54** 4864
[14] Daw M S and Baskes M I 1983 *Phys. Rev. Lett.* **50** 1285
[15] Foiles S M, Baskes M I and Daw M S 1986 *Phys. Rev.* B **33** 7983
[16] Foiles S M and Daw M S 1987 *J. Mater. Res.* **2** 5
[17] Gehlen P C, Hahn G T and Kanninen M F 1972 *Scr. Metall.* **6** 1087
[18] Kohlhoff S 1988 *Proc. Int. Finite-Element Method Congr. (Baden-Baden, Germany, 1988)* (Stuttgart: IKOSS)
[19] Kohlhoff S, Gumbsch P and Fischmeister H F 1991 *Phil. Mag.* A **64** 851
[20] Ohr S M 1985 *Mater. Sci. Eng.* **72** 1
[21] Chiao Y-H and Clarke D R 1989 *Acta Metall.* **37** 203
[22] Wang J-S and Anderson P M 1991 *Acta Metall.* **39** 779
[23] Wang J-S and Beltz G E 1992 *Acta Metall.* **40** 1675
[24] Zhou S J, Carlsson A E and Thomson R 1993 *Phys. Rev.* B **47** 7710
[25] Zhou S J, Carlsson A E and Thomson R 1994 *Phys. Rev. Lett.* **72** 852
[26] Thomson R and Carlsson A E 1994 *Phil. Mag.* A **70** 893
[27] Sun Y, Beltz G E and Rice J R 1993 *Mater. Sci. Eng.* A **170** 67
[28] Sun Y and Beltz G E 1994 *J. Mech. Phys. Solids* **42** 1905
[29] Sun Y and Rice J R 1995 unpublished work
[30] Hoagland R G and Heinisch H L *J. Mater. Res.* **7** 2080
[31] Gumbsch P 1995 *J. Mater. Res.* at press
[32] Kröner E 1967 *Int. J. Solids Struct.* **3** 731
[33] Sih G C and Liebowitz H 1968 *Fracture* vol 2, ed H Liebowitz (New York: Academic) ch 2, p 67
[34] Fletcher R and Reeves C M 1964 *Comput. J.* **7** 149
[35] Polak E 1971 *Computational Methods in Optimization* (New York: Academic)
[36] Thomson R, Hsieh C and Rahna V 1971 *J. Appl. Phys.* **42** 3154
[37] Mullins M 1984 *Int. J. Fract.* **24** 189
[38] Baskes M I and Daw M S 1990 *Proc. 4th Int. Conf. on the Effect of Hydrogen on the Behavior of Materials (Jackson Lake Lodge, WY, 1990)* (Warrendale, PA: Metallurgical Society of AIME)
[39] Peierls R E 1940 *Proc. Phys. Soc.* **52** 34
[40] Nabarro F R N 1947 *Proc. Phys. Soc.* **59** 256
[41] Atkinson C 1966 *Int. J. Fract. Mech.* **2** 567
[42] Asaro R J 1975 *J. Phys. F: Met. Phys.* **5** 2249
[43] Suo Z 1990 *Proc. R. Soc.* A **427** 331
[44] Erdogan F and Gupta G D 1972 *Quart. Appl. Math.* **29** 525
[45] Rice J R and Beltz G E 1994 *J. Mech. Phys. Solids.* **42** 333
[46] Xu G, Argon A S and Ortiz M 1995 *Phil. Mag.* A at press
[47] Beltz G E, Rice J R, Shih C F and Xia L 1995 *Acta Metall.* at press
[48] Lipkin D M and Beltz G E 1995 *Acta Metall.* at press
[49] Beltz G E and Schmauder S 1994 *Defect–Interface Interactions (Mater. Res. Sci. Symp. 319) (Boston, MA, 1993)* ed E P Kvam, A H King, M J Mills and V Vitek (Pittsburgh, PA: Materials Research Society)
[50] Gumbsch P and Beltz G E 1995 unpublished work
[51] Schoeck G 1995 *J. Mech. Phys. Solids* at press
[52] Mesarovic S Dj and Beltz G E 1995 unpublished work
[53] Carlsson A E, Thomson R, Beltz G E and Gann L 1995 unpublished work
[54] Schoeck G and Püschl W 1991 *Phil. Mag.* A **64** 931